INSTITUTE OF PHYSICS PUBLISHING EUROPEAN JOURNAL OF PHYSICS

Eur. J. Phys. **22** (2001) 169–184 www.iop.org/Journals/ej PII: S0143-0807(01)14580-0

Teaching astronomical speckle techniques

Claude Aime

UMR 6525 Astrophysique, Faculté des Sciences de l'Université de Nice Sophia-Antipolis, Parc Valrose-06108, Nice Cedex 2, France

Received 7 June 2000, in final form 6 December 2000

Abstract

This paper gives an introduction to speckle techniques developed for high angular-resolution imagery in astronomy. The presentation is focussed on fundamental aspects of the techniques of Labeyrie and Weigelt. The formalism used is that of Fourier optics and statistical optics, and corresponds to graduate level. Several new approaches of known results are presented. An operator formalism is used to identify similar regions of the bispectrum. The relationship between the bispectrum and the phase closure technique is presented in an original geometrical way. Effects of photodetection are treated using simple Poisson statistics. Realistic simulations of astronomical speckle patterns illustrate the presentation.

1. Introduction

In the absence of atmospheric turbulence, the wave coming from a point source arrives at a telescope in the form of a plane wave. The wave forms an interference pattern at the focus given by the modulus squared of the Fourier transform of the aperture transmission. This pattern is called the point-spread function (PSF); for a perfect telescope, it is the Airy function, of angular size λ/D, where λ is the wavelength of the light and D is the diameter of the telescope aperture. The theoretical width of the PSF of an 8 m telescope in the visible range should be about 0.015 arc s. However, in the presence of turbulence, a classical observation made with that telescope will show a large PSF, typically of 1 arc s.

Labeyrie [1] shows that the instantaneous image at the focus of a large ground-based telescope resembles the speckle pattern observed in optics with a laser and a diffuser. The image corresponds to the interference of the wavefront perturbed by the variations of the optical path through the atmosphere. An illustration of such a wavefront and the corresponding speckle image is given in figure 1. Speckles appear as an ensemble of small spots the size of the Airy disc that spread over a zone of angular diameter λ/r_0, where r_0 is the parameter introduced by Fried [2] to measure the strength of the turbulence. The parameter r_0 gives the characteristic size of the wavefront perturbations. The speckle pattern continually changes over time, giving the impression of a boiling structure, with a typical lifetime of 5 ms. The observation of speckle patterns therefore requires very short time exposures to freeze the atmospheric turbulence. A long time exposure blurs the speckles and leaves a large and smooth long-time-exposure PSF.

0143-0807/01/020169+16$30.00

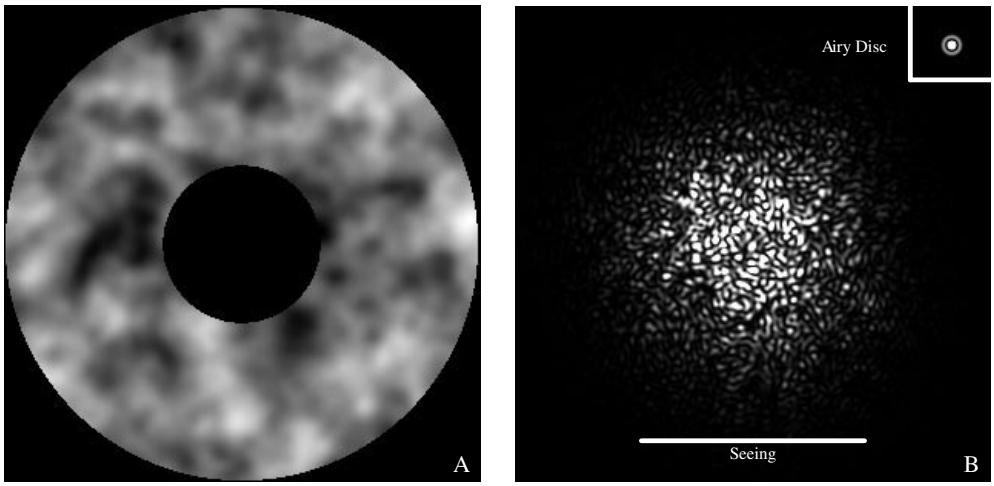

Figure 1. Grey-level representation of the wavefront at the telescope aperture (A) and its corresponding speckle pattern (B) in the focal plane. The wavefront is the result of a numerical simulation that consists of filtering a white noise (generated as an ensemble of random numbers) by a low-pass filter. Here the filter follows the model of von-Karman, with an inner and outer scale of turbulence [10], but any low-pass filter correctly chosen may produce acceptable simulated speckle patterns. Individual speckles have the size λ/D of the Airy disc of the telescope (upper-right corner). The line gives the characteristic size λ/r_0 of the 'seeing'.

A speckle pattern shows roughly $n_S \approx (D/r_0)^2$ speckles. A typical value for r_0 is 10 cm at 500 nm; this makes more than 5000 speckles for an 8 m telescope in the visible range. The pattern is wavelength dependent, and narrow spectral bandwidths (typically 10 nm in the visible) must be used. There are fewer speckles in the infrared than in the visible and r_0 increases in size with the wavelength as $\lambda^{1.2}$. A detailed analysis of the effects of atmospheric turbulence on the observations can be found in the review by Roddier [3].

Labeyrie [1] proposed to take advantage of speckle patterns for high-angular imaging in astronomy. His work initiated a considerable number of studies in astronomical imaging [4, 5]. In this paper, besides the presentation of Labeyrie's original speckle interferometry technique (section 3), we very briefly outline the technique of Knox and Thompson [6] (section 4) and describe in more detail the speckle masking technique of Weigelt [7] (section 5). All these techniques use statistical analyses of the image and recover information up to the theoretical diffraction limit of the telescope.

It should be pointed out that at present, speckle-imaging techniques find a serious challenger in adaptive optics techniques[1], which try to correct in real time the perturbed wavefront and have given important results in the infrared. Speckle techniques remain interesting however, for visible wavelengths observations, for the very large telescopes planned in the near future and also for smaller telescopes operated with low-level technology. They can be used at very low light levels, when only a few photoelectrons per image are recorded, provided a very large number of images are processed. A detailed analysis of the effect of photodetection is made in section 6, by means of simple Poisson statistics.

The presentation in this paper is focussed on fundamental aspects that may constitute an interesting field of application for Fourier optics, statistics and photodetection processes learned by students at the graduate level. The numerical illustrations that are given throughout the paper to illustrate the equations and results are made with *Mathematica* [9] and can be easily reproduced with a PC.

[1] For adaptive optics see, for example, [8].

2. Image formation at the focus of a large ground-based telescope

For an astronomical object $o(r)$ of small angular extent, an identical point spread function (PSF) $s(r)$ may be assumed for the whole field, and the image observed in the focal plane of the telescope is given by the convolution relation:

$$f(r) = \int o(x)s(r-x)\,\mathrm{d}x = s(r) \otimes o(r) \tag{1}$$

where the symbol $\otimes$ denotes the convolution.

It is important to note that $s(r)$ is a random function, which varies from one image to another. Fourier optics [11] shows that $s(r)$ is proportional to the modulus squared of the Fourier transform of the complex amplitude of the wave at the aperture of the telescope:

$$s(r) = |\mathfrak{F}_{r,r/\lambda}[P(r)]|^2 \tag{2}$$

where $P(r) = P_0(r)\Psi(r)$ is the product the aperture of the telescope $P_0(r)$ and the complex function $\Psi(r)$ that represents the effects of the atmospheric turbulence on the instantaneous incident wavefront. The pupil function $P_0(r)$ may eventually be complex to take into account fixed aberrations of the optics. The symbol $\mathfrak{F}$ denotes the operator of Fourier transformation, the indices give the variable names before and after the transformation is applied, so that

$$\mathfrak{F}_{r,u}[f(r)] = \int f(r)\,\mathrm{e}^{-2\mathrm{i}\pi ur}\,\mathrm{d}r = F(u). \tag{3}$$

With this convention, the Fourier transform of (2) is a function of the angular 'frequency' value r/λ, or simply of r if we express the aperture in units of wavelength, which we shall do here. The effects of speckle patterns on the image can also be described in the Fourier plane. Taking the Fourier transform of (1), and using capital letters to denote the Fourier transformation, we have

$$F(u) = S(u)O(u) \tag{4}$$

where $S(u)$ is the random optical transfer function (OTF) that can be written as the autocorrelation function of the complex amplitude of the wave on the telescope aperture:

$$S(u) = \frac{1}{A}\int P_0(r)\Psi(r)P_0^*(r-u)\Psi^*(r-u)\,\mathrm{d}r \tag{5}$$

where * stands for complex conjugate and A is a normalization factor equal to the surface area of the aperture. The OTF equals one at the zero spatial frequency, falls rapidly over a frequency range of r_0/λ and becomes an irregular complex function up to the telescope cut-off frequency D/λ. Outside very low frequencies, the modulus of $S(u)$ resembles a speckle pattern with 'frequency speckles' of size r_0/λ different from one image to another. There is on average a 2π phase variation within a frequency speckle. An illustration of $S(u)$ is given in figure 2.

3. Labeyrie's speckle interferometry technique

Labeyrie's technique permits the modulus of the Fourier transform $O(u)$ of the astronomical object to be obtained up to the telescope cut-off frequency. The phase of $O(u)$ is not recovered, only the autocorrelation of the object can be reconstructed, not the object itself. This information is generally enough for measuring star diameters and double-star separations.

The speckle interferometry technique requires the computation of the power spectrum $W_f(u)$ of the speckled image $f(r)$ or of its autocorrelation function $C_f(\rho)$. These statistical functions are defined by:

$$C_f(\rho) = \langle \int f(r)f(r+\rho)\,\mathrm{d}r \rangle = \langle f(\rho) \otimes f(-\rho) \rangle \qquad W_f(u) = \langle |F(u)|^2 \rangle \tag{6}$$

where $\langle \ldots \rangle$ denotes an ensemble average.

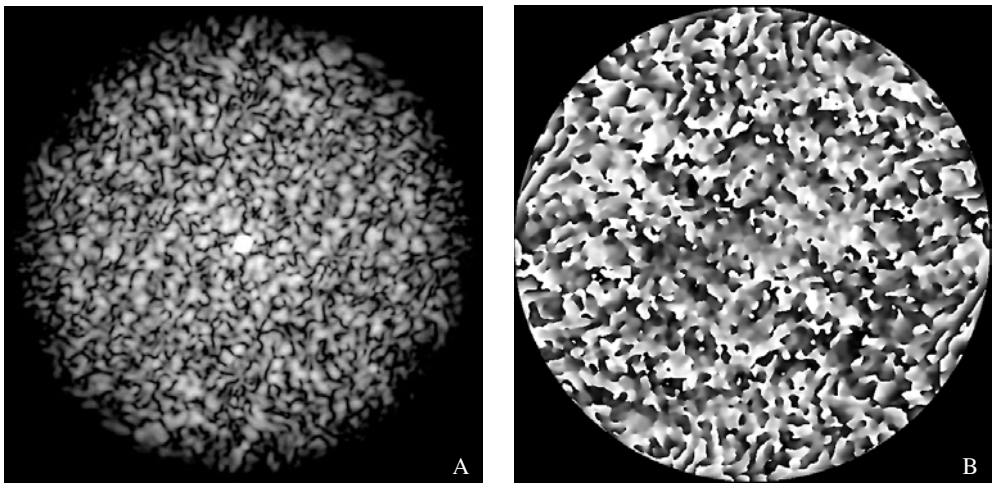

Figure 2. Fourier space: logarithm of the modulus of the OTF (A) and phase (B) of the Fourier transform of the speckle pattern shown in figure 1(B). The zero spatial frequency is at the centre of the image and the OTF extends over a circular area of diameter $2D/\lambda$. The bright central part of (A) corresponds to the very low frequencies transmitted in a long-time-exposure experiment. The OTF presents itself a speckled form of characteristic size r_0/λ.

The Wiener–Khinchin theorem shows that $W_f(u)$ and $C_f(\rho)$ are Fourier transform pairs. This can be easily demonstrated taking the Fourier transform $\mathfrak{F}_{\rho,u}$ of the autocorrelation function:

$$\mathfrak{F}_{\rho,u}[\langle \int f(r)\,f(r+\rho)\,\mathrm{d}r\rangle] = \langle \int f(r)\mathfrak{F}_{\rho,u}[f(r+\rho)]\,\mathrm{d}r\rangle = \langle F(u)\int f(r)\,\mathrm{e}^{2\mathrm{i}\pi ur}\,\mathrm{d}r\rangle$$
$$= \langle F(u)F(-u)\rangle = \langle |F(u)|^2\rangle \qquad \text{or} \qquad \mathfrak{F}_{\rho,u}[C_f(\rho)] = W_f(u). \tag{7}$$

Several useful rules have been used here. One is that the ensemble average, spatial integration and Fourier transform are linear operations whose order of application can be permuted. Another is that $\mathfrak{F}_{\rho,u}$ applies directly to the function of ρ, $f(r+\rho)$ for which r is a constant, so that $\mathfrak{F}[f(r+\rho)] = F(u)\,\mathrm{e}^{2\mathrm{i}\pi ru}$. We finally used the fact that $F(-u) = F^*(u)$ since $f(r)$ is real. The demonstration of the Wiener–Khinchin theorem is even faster if one takes the Fourier transform of $\langle f(\rho)\otimes f(-\rho)\rangle$ and uses the properties of the Fourier transform relative to the convolution. However, the demonstration given in relation (7) remains interesting from a pedagogic point of view. It generalizes straightforwardly to higher orders, in particular to the triple correlation function that will be used in Weigelt's technique (section 5).

A practical implementation of Labeyrie's technique consists of recording a large number of short-exposure images to obtain a good estimate of the ensemble average of relation (6). Two series of observations are necessary to remove the effect of the atmosphere, one on the astronomical object and another on an unresolved star. The linear relation between $F(u)$, $S(u)$ and $O(u)$ described by equation (4) permits us to obtain the square of the modulus of $O(u)$ from the ratio of the two power spectra:

$$|O(u)|^2 = \frac{W_f(u)}{W_s(u)} \qquad \text{with} \qquad W_s(u) = \langle |S(u)|^2\rangle \tag{8}$$

The quantity $W_s(u)$ is the telescope–atmosphere energy transfer function (ETF). It is non-zero up to the theoretical frequency cut-off of the telescope for a perfect instantaneous monochromatic image. This result can be deduced from the shape of the instantaneous OTF (figure 2). Many studies have been made to determinate the exact shape of the telescope–atmosphere ETF; in the high frequencies well outside r_0/λ, it is roughly equal to the OTF of

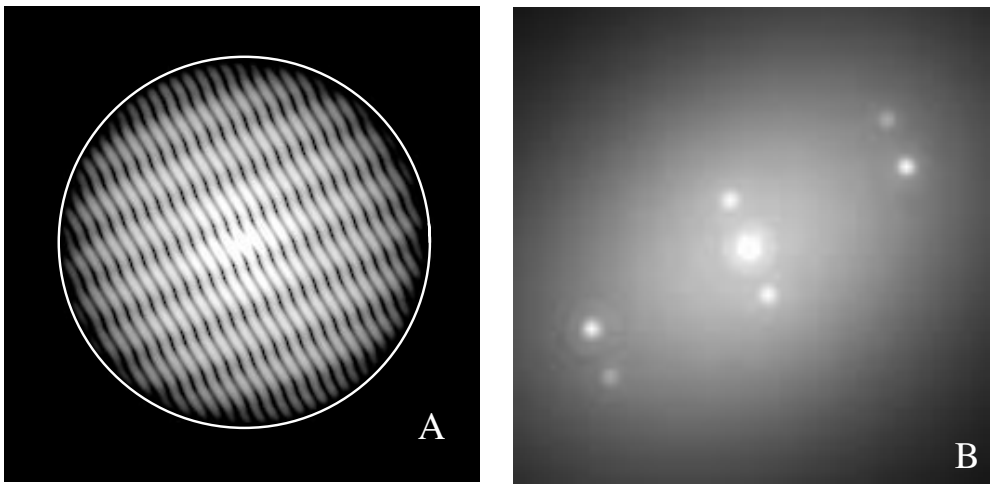

Figure 3. (A) Representation on a logarithmic scale of the power spectrum $W_f(u)$ obtained from a data set of 100 simulated speckle images of a triple star of intensities proportional to 1, 0.7 and 0.4. For each image, a speckle pattern $s(r)$ similar to that of figure 1(B) is first computed; three identical weighted and shifted images of $s(r)$ are then added to give the triple-star speckle pattern. The stars (not resolved individually) give rise to fringe patterns up to the telescope cut-off frequency (bright circle). Two of the three fringe patterns are clearly visible, the third appears by tilting the image and viewing it at low angles. (B) Central part of the autocorrelation function $C_f(\rho)$ clearly showing the seven points of the triple star autocorrelation function.

a perfect telescope divided by the number of speckles n_S [3]. Its precise shape is in fact more complicated, and depends in a non-separable manner of the telescope and the atmospheric conditions. In practice, if a reference star is used, caution must be taken with regard to rapid variations in the atmospheric turbulence when performing the calibration defined by relation (8). The usual procedure is to alternatively observe the astronomical object and the reference and to combine data obtained under similar atmospheric conditions.

Labeyrie's speckle interferometry technique is primarily of interest for measuring star diameters and double- or multiple-star separations. A numerical noiseless illustration of the technique is shown in figure 3 for a triple star. The triple star produces fringe patterns in the power spectrum (figure 3(A)). Its signature in the image autocorrelation is made of seven points, clearly visible in figure 3(B).

For real data contaminated by noise, the observation of a double star with large magnitude differences needs elaborate treatment, and it is generally assumed that a maximum of five magnitudes difference is the limit of detection. Stellar diameter measurement is an even tougher problem.

Since the modulus alone of $O(u)$ can be retrieved, and not its phase, the speckle interferometry technique is not strictly speaking an imaging technique. Fienup [12] proposed an iterative procedure that tends to recover the unknown phase by the successive application of constraints in the real and Fourier planes. This procedure requires very precise measurements and reconstructs objects $o(r)$ whose modulus of the Fourier transforms are equal to $|O(u)|$, but a unique solution for $o(r)$ is not guaranteed: two different objects may have an identical modulus of the Fourier transform.

4. The technique of Knox and Thompson

Shortly after Labeyrie's original proposal, Knox and Thompson [6] proposed a generalization of his technique that allows phase reconstruction. We briefly describe this technique, which is

also closely related to the speckle masking technique. The technique of Knox and Thompson consists of computing the quantity

$$K_f(u, \Delta) = \langle F(u)F^*(u+\Delta)\rangle \tag{9}$$

where Δ is a small frequency variation. Using relation (4), we can write

$$K_f(u, \Delta) = O(u)O^*(u+\Delta)K_s(u, \Delta). \tag{10}$$

The quantity $K_s(u, \Delta)$ is real and positive if Δ is very small compared with r_0/λ, i.e. u and $u+\Delta$ belong to the same speckle of the Fourier plane. Writing $S(u) = M(u)\exp(\mathrm{i}A(u))$, and assuming statistical independence between modulus and phase, we have

$$K_s(u, \Delta) = \langle S(u)S^*(u+\Delta)\rangle = \langle M(u)M(u+\Delta)\rangle\langle \mathrm{e}^{\mathrm{i}(A(u)-A(u+\Delta)}\rangle. \tag{11}$$

With $\Delta \ll r_0/\lambda$ we can make the approximation $M(u+\Delta) \approx M(u)$ and assure that the phase difference $A(u) - A(u+\Delta)$ is small compared with 2π. Then, using the approximation $\mathrm{e}^{\mathrm{i}\theta} \approx 1+\mathrm{i}\theta$, and assuming $\langle A(u)-A(u+\Delta)\rangle = 0$, we can derive $K_s(u, \Delta) \approx W_s(u)$. Denoting the phase of $O(u)$ by $\phi(u)$, the phase of $K_f(u, \Delta)$ gives the phase difference $\phi(u)-\phi(u+\Delta)$. The complete value of $O(u)$ may therefore be reconstructed from summed differences.

5. Weigelt's speckle masking technique

5.1. Principle of the technique

Weigelt 's technique is based on the computation of the image triple correlation function and its Fourier transform, the bispectrum.

The triple correlation function $T_f(\rho_1, \rho_2)$ of $f(r)$ is defined by

$$T_f(\rho_1, \rho_2) = \langle \int f(r)f(r+\rho_1)f(r+\rho_2)\,\mathrm{d}r\rangle. \tag{12}$$

The bispectrum $B_f(u_1, u_2)$ is the Fourier transform of the triple correlation function; the terms triple(correlation) and bi(spectrum) used to denote corresponding functions are obviously inconsistent, but widely used and are kept here.

Denoting, for conciseness of writing, by $\mathfrak{F}_1$ and $\mathfrak{F}_2$ the Fourier transforms that are applied to the functions of ρ_1 and ρ_2 giving functions of u_1 and u_2, we have

$$\begin{aligned}\mathfrak{F}_1\mathfrak{F}_2[C_f(\rho_1, \rho_2)] &= \langle \int f(r)\mathfrak{F}_1[f(r+\rho_1)]\mathfrak{F}_2[f(r+\rho_2)]\,\mathrm{d}r\rangle \\ &= \langle F(u_1)F(u_2)\int f(r)\,\mathrm{e}^{2\mathrm{i}\pi(u_1+u_2)r}\,\mathrm{d}r\rangle = \langle F(u_1)F(u_2)F(-u_1-u_2)\rangle \\ \text{or} \qquad B_f(u_1, u_2) &= \langle F(u_1)F(u_2)F^*(u_1+u_2)\rangle. \end{aligned} \tag{13}$$

In principle, a simple compensation of the effects of the atmospheric turbulence is also possible here. Replacing $F(u)$ by $S(u)O(u)$ in the expression of the bispectrum, we can write

$$B_O(u_1, u_2) = O(u_1)O(u_2)O^*(u_1+u_2) = \frac{B_f(u_1, u_2)}{B_s(u_1, u_2)} \tag{14}$$

where $B_s(u_1, u_2) = \langle S(u_1)S(u_2)S^*(u_1+u_2)\rangle$ is the bispectrum transfer function. Assuming, as we shall discuss later, that $B_s(u_1, u_2)$ is a real positive quantity that may be obtained using an unresolved star, one can recover the bispectrum of the object alone, or equivalently its triple correlation.

The object bispectrum is a complex quantity that retains the information on the shape of $o(r)$. This can be readily shown in the triple correlation function using a presentation similar to Lohmann *et al* [13]. The reader may verify that the object triple correlation of relation (14) can also be written as the convolution product $o(\rho_2)o(\rho_2+\rho_1) \otimes o(-\rho_1)$ that applies to

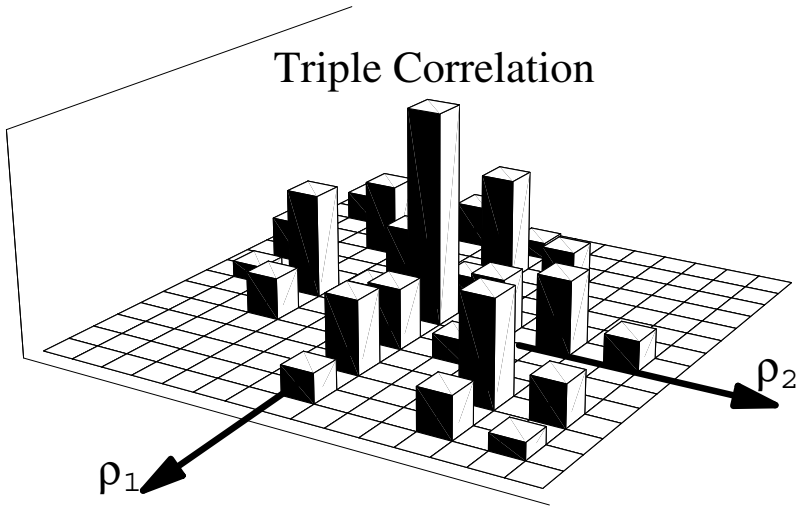

Figure 4. Triple correlation function of a one-dimensional object. The object, made of three unresolved stars of values proportional to 4, 10 and 7, appears at the edges of the figure. This result may be easily obtained by drawing the object on 3 sheets of paper (here the triple star is represented by holes). The diagram corresponding to $o(r)$ is maintained fixed and the others representing $o(r+\rho_1)$ and $o(r+\rho_2)$ are shifted according to ρ_1 and ρ_2 values. Using for ρ_1 a displacement equal to the separation between extreme points, the quantity $o(r)o(r+\rho_1)$ makes a 'mask' that is used to see the image $o(r+\rho_2)$ that is swept over. The same procedure may be applied to two-dimensional images using transparencies (see figures 2 and 4 of [13]).

functions of ρ_1. For particular values of ρ_1 this is called the 'masking vector', from which the name of the technique originates, $o(\rho_2)o(\rho_2+\rho_1)$ becomes similar to a Dirac delta function and the convolution product gives back the object $o(r)$. There are several values of ρ_1 that can give this result. An illustration of this property is made in figure 4, which presents the triple correlation function of a one-dimensional image.

The practical implementation of the technique consists of the phase reconstruction in the Fourier plane. Denoting as above the phase of $O(u)$ by $\phi(u)$, the phase of $B_O(u_1+u_2)$ equals $\phi(u_1)+\phi(u_2)-\phi(u_1+u_2)$. The phase of $O(u)$ at a given frequency u can then be recovered from bispectral phases at frequency positions u_1 and u_2 so that $u=u_1+u_2$. A recursive method can be worked out [14]. The method leads to the recovery of the phase of $O(u)$ with an unknown additive phase term that corresponds to an uncertainty in the object position. This could be expected since the triple correlation function, as the autocorrelation function, is insensitive to the translation of an object.

5.2. Symmetries of the bispectrum

For a telescope of diameter D operated at the wavelength λ, the optical transfer function $S(u)$ has a cut-off frequency D/λ; the support of the bispectrum in the $\{u_1,u_2\}$ plane is defined by the set of inequalities $|u_1|\leqslant D/\lambda$, $|u_2|\leqslant D/\lambda$ and $|u_1+u_2|\leqslant D/\lambda$. For a one-dimensional signal this corresponds to the hexagon shown in figure 5.

Such a hexagon is divided into six regions by the lines $u_1=0$, $u_2=0$ and $u_1+u_2=0$ for which the bispectrum reduces to Labeyrie's technique. Indeed, for these values $B_f(u_1,u_2)$ of relation (13) reduces to the power spectrum of relation (6) since $F(0)=F^*(0)=1$. Next to these lines, a narrow strip is similar to the Knox–Thompson technique. Making $u_2=\Delta$, with $\Delta\ll r_0/\lambda$ we can assume that $F(\Delta)\approx 1$, and the term $\langle F(u_1)F^*(u_1+\Delta)\rangle$ of relation (9) appears.

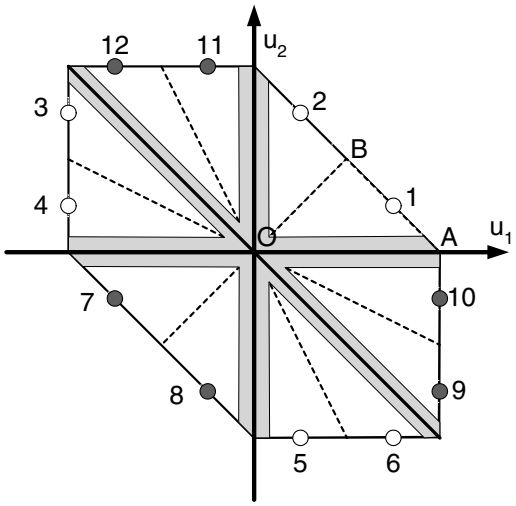

Figure 5. Illustration of symmetries of the bispectrum for a one-dimensional band-limited signal. The bold lines correspond to Labeyrie's technique. Close-by regions are almost equivalent to the technique of Knox and Thompson (see section 5.2). The reader may verify that the six transformations ($\mathbf{T}_1$ to $\mathbf{T}_6$) of relation (18) applied to point 1 of the fundamental triangle OAB give points 1 to 6. As shown in (15), the bispectrum is the same for these points. The complex conjugate value is found for a second set of centrally opposite points (numbered 7 to 12). Degeneracy occurs at the edges of the segment AB. When point 1 meets A, the bispectrum is real and points of the first and second sets merge with their closest neighbour (1 with 10, 2 with 11, and so on). The images of A are the vertices of the hexagon. When point 1 meets B, the six points of the first set merge to leave only three points (1 merges with 2, 3 with 4 and 5 with 6). These points and their opposite points are the midpoints of the sides of the hexagon. Varying the distance of point 1 to the centre O, this reasoning shows that the whole information of the bispectrum is contained in the fundamental triangle OAB.

It has been shown [15] that it is enough to compute the bispectrum for the basic triangle *OAB* in figure 5; simple reasoning can show this. The total number of the transformations in the $\{u_1, u_2\}$ plane that leave $B(u_1, u_2)$ unchanged are those that correspond to the six permutations of the three elements $F(u_1)$, $F(u_2)$ and $F(-u_1 - u_2)$. For example, three out of six of these permutations are written below:

$$B(u_1, u_2) = \langle F(u_1)F(u_2)F(-u_1 - u_2)\rangle \tag{15a}$$

$$B(u_1, u_2) = \langle F(u_2)F(u_1)F(-u_2 - u_1)\rangle \tag{15b}$$

or

$$B(u_1, u_2) = \langle F(u_1 - u_2)F(u_2)F(u_1)\rangle \tag{15c}$$

where (15*a*) is the original term, (15*b*) is the term in which $F(u_1)$ is replaced by $F(u_2)$ and (15*c*) the term in which $F(u_1)$ is replaced by $F(-u_1 - u_2)$. The transformations are linear and can be interpreted in terms of classical geometry. Transformation (15*b*) $\{u_1 \to u_2, u_2 \to u_1\}$ represents a reflection at the axis $u_2 = u_1$ and transformation (15*c*) $\{u_1 \to -u_1 - u_2, u_2 \to u_2\}$ corresponds to a sheared reflection at the axis $u_2 = -2u_1$.

The problem may be presented easily by means of operators. The transformation matrices are a matrix of symmetry **S** and a pseudo-shear matrix **C** for transformation (15*b*) and (15*c*) respectively:

$$\mathbf{S} = \begin{bmatrix} 0 & 1 \\ 1 & 0 \end{bmatrix} \qquad \mathbf{C} = \begin{bmatrix} -1 & -1 \\ 0 & 1 \end{bmatrix}. \tag{16}$$

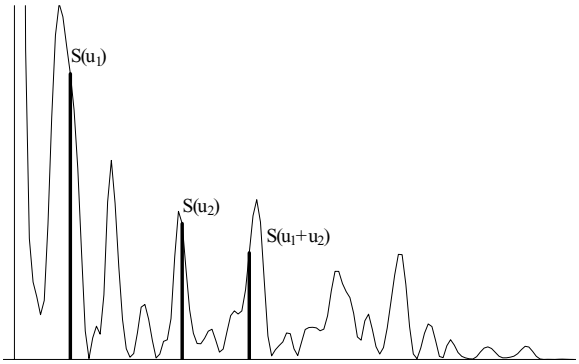

Figure 6. Modulus of $S(u)$ represented on a linear scale, with a plot range sufficient to make the speckles on the frequency plane visible (it is a radial cut of figure 2). $S(u_1)$, $S(u_2)$ and $S(u_1+u_2)$ clearly belong to different speckles. However these functions are not independent RV_s, and the bispectrum $B_S(u_1, u_2)$ is not zero outside the regions corresponding to the techniques of Labeyrie and Knox and Thompson (section 5.3). The figure may be used to show that by making u_1, u_2 or u_1+u_2 equal to zero or Δ, one recovers these later techniques as described in section 5.2.

Denoting the identity matrix by '**I**', the six permutations of terms in the bispectrum $B(u_1, u_2)$ may be obtained by combining operations **C** and **S** in the following six combinations:

$$\mathbf{T}_1 = \mathbf{I} \qquad \mathbf{T}_2 = \mathbf{S} \qquad \mathbf{T}_3 = \mathbf{C}\cdot\mathbf{S} \qquad \mathbf{T}_4 = \mathbf{C} \qquad \mathbf{T}_5 = \mathbf{S}\cdot\mathbf{C}$$
$$\text{and} \qquad \mathbf{T}_6 = \mathbf{S}\cdot\mathbf{C}\cdot\mathbf{S} \tag{17}$$

where the dot $(\cdot)$ denotes a product of matrices. We then have

$$\mathbf{T}_1 = \begin{bmatrix} 1 & 0 \\ 0 & 1 \end{bmatrix} \qquad \mathbf{T}_2 = \begin{bmatrix} 0 & 1 \\ 1 & 0 \end{bmatrix} \qquad \mathbf{T}_3 = \begin{bmatrix} -1 & -1 \\ 1 & 0 \end{bmatrix}$$
$$\mathbf{T}_4 = \begin{bmatrix} -1 & -1 \\ 0 & 1 \end{bmatrix} \qquad \mathbf{T}_5 = \begin{bmatrix} 0 & 1 \\ -1 & -1 \end{bmatrix} \qquad \mathbf{T}_6 = \begin{bmatrix} 1 & 0 \\ -1 & -1 \end{bmatrix}. \tag{18}$$

The result of the application of these transformations to a point of the bispectrum is shown in figure 5. The transformation order is chosen here so that a point of the fundamental triangle *OAB* rotates anticlockwise.

Now, using the Hermitian property of the transform ($B(-u_1, -u_2) = B^*(u_1, u_2)$), we can add six more plane transformations

$$\mathbf{T}_7 = -\mathbf{T}_1 \qquad \mathbf{T}_8 = -\mathbf{T}_2 \qquad \mathbf{T}_9 = -\mathbf{T}_3 \qquad \mathbf{T}_{10} = -\mathbf{T}_4 \qquad \mathbf{T}_{11} = -\mathbf{T}_5$$
$$\text{and} \qquad \mathbf{T}_{12} = -\mathbf{T}_6. \tag{19}$$

Applying these new transformations to point 1, we obtain six new points numbered 7 to 12. The determinant of all these matrices is either 1 or -1, and the areas are therefore conserved. The 12 transformations make it possible to recover the hexagon from the fundamental triangle.

The formalism developed here can be generalized to the trispectrum, a quantity that has found applications in signal processing.

5.3. Bispectrum and phase closure

An important question remains: is $B_S(u_1, u_2)$ non-zero for whatever the values of u_1 and u_2 are that lie outside regions similar to Labeyrie's and Knox and Thompson's techniques? There is a strong temptation to answer that $\langle S(u_1)S(u_2)S^*(u_1+u_2)\rangle$ should be zero. If we assume that u_1, u_2 and u_1+u_2 correspond to points inside different frequency speckles (figure 6), we might consider that $S(u_1)$, $S(u_2)$ and $S^*(u_1+u_2)$ are independent random variables (RVs). Making use of the property that for independent RVs the average product equals the product

average, the bispectrum reduces to $\langle S(u_1)\rangle\langle S(u_2)\rangle\langle S^*(u_1+u_2)\rangle$. This quantity falls to zero for u large compared to r_0/λ since each term reduces to the long-time-integration OTF. This simple reasoning is wrong; $S(u_1)$, $S(u_2)$ and $S^*(u_1+u_2)$ depend on the phase of the same telescope aperture and the assumption of independence is not verified.

We give below the correct answer to this problem. The approach is derived from Ayers *et al* [16] and Roddier [17], who first noticed the relationship between the bispectrum and the phase closure technique.

Let us start with the simplest aperture that can give terms in the fundamental triangle outside the axes. Such an aperture $P_o(r)$ is that of a small interferometer with three elementary telescopes (I3T). The reader may verify that a two-telescope interferometer (I2T) gives only contributions along the axes. To make things as simple as possible, I assume that the apertures of the I3T are on a line and spaced in a non-redundant way, with separations equal to d and $2d$. The elementary apertures are small enough to assume a constant phase over each elementary aperture $\pi(r)$. The transmission $P(r)$ of the I3T may be written as

$$P(r) = \mathrm{e}^{\mathrm{i}\theta_1}\pi(r) + \mathrm{e}^{\mathrm{i}\theta_2}\pi(r-d) + \mathrm{e}^{\mathrm{i}\theta_3}\pi(r-3d) \tag{20}$$

where θ_1, θ_2 and θ_3 are phase terms due to atmospheric turbulence.

Using (5), the OTF becomes

$$\begin{aligned} S(u) = \Delta(u) + \tfrac{1}{3}\{&\mathrm{e}^{\mathrm{i}(\theta_2-\theta_1)}\Delta(u-d) + \mathrm{e}^{\mathrm{i}(\theta_3-\theta_2)}\Delta(u-2d) + \mathrm{e}^{\mathrm{i}(\theta_3-\theta_1)}\Delta(u-3d) \\ &+ \mathrm{e}^{-\mathrm{i}(\theta_2-\theta_1)}\Delta(u+d) + \mathrm{e}^{-\mathrm{i}(\theta_3-\theta_2)}\Delta(u+2d) + \mathrm{e}^{-\mathrm{i}(\theta_3-\theta_1)}\Delta(u+3d)\} \end{aligned} \tag{21}$$

where $\Delta(u)$ is the autocorrelation function $\pi(u)\otimes\pi(-u)$ of the elementary pupil. Note that (21) may also be easily verified graphically by drawing $P(r)$ and $P^*(r)$ on two sheets of paper and displacing them.

Let us very briefly consider relation (21) from the point of view of phase closure, a technique that comes from radio astronomy. The telescope transmits the frequencies u_{12}, u_{23} and u_{13} corresponding to the separations between the three elementary apertures (here d, $2d$ and $3d$), with atmospheric phase errors $\theta_2-\theta_1$, $\theta_3-\theta_2$ and $\theta_3-\theta_1$. These atmospheric phase errors disappear if we form the sum of phases at frequencies u_{12} and u_{23} minus the phase at u_{13}; this effect is known as phase closure. We will rediscover this property directly from the bispectrum.

For simplicity of writing we replace $\Delta(u)$ in relation (21) by the Dirac delta function $\delta(u)$; the reader may eventually continue the same reasoning with full apertures.

The terms $S(u_1)$, $S(u_2)$ and $S^*(u_1+u_2)$ that contribute to the fundamental triangle of the bispectrum may be written as

$$\begin{aligned} S(u_1) &= \delta(u_1) + \tfrac{1}{3}[\mathrm{e}^{\mathrm{i}(\theta_2-\theta_1)}\delta(u_1-d) + \mathrm{e}^{\mathrm{i}(\theta_3-\theta_2)}\delta(u_1-2d) + \mathrm{e}^{\mathrm{i}(\theta_3-\theta_1)}\delta(u_1-3d)] \\ S(u_2) &= \delta(u_2) + \tfrac{1}{3}[\mathrm{e}^{\mathrm{i}(\theta_2-\theta_1)}\delta(u_2-d) + \mathrm{e}^{\mathrm{i}(\theta_3-\theta_2)}\delta(u_2-2d) + \mathrm{e}^{\mathrm{i}(\theta_3-\theta_1)}\delta(u_2-3d)] \\ S^*(u_1+u_2) &= \delta(u_1+u_2) + \tfrac{1}{3}[\mathrm{e}^{-\mathrm{i}(\theta_2-\theta_1)}\delta(u_1+u_2-d) + \mathrm{e}^{-\mathrm{i}(\theta_3-\theta_2)}\delta(u_1+u_2-2d) \\ &\quad + \mathrm{e}^{-\mathrm{i}(\theta_3-\theta_1)}\delta(u_1+u_2-3d)]. \end{aligned} \tag{22}$$

One may substitute these three terms in the bispectrum, and use the properties of the Dirac delta function. Alternatively a simple geometrical solution may be worked out. In the $\{u_1, u_2\}$ plane, the Dirac delta functions may be represented as straight lines (figure 7). For example, $\delta(u_1+u_2-d)$ is a function that is zero everywhere but for $u_1+u_2=d$. For the fundamental triangle, the quantity $S(u_1)$ appears as four vertical lines (at $u_1=0$, d, $2d$ and $3d$), with phase terms ($\theta_2-\theta_1$, $\theta_3-\theta_2$, etc) written in figure 7. The straight line at $u_1=0$ merges with the vertical axis, and has no phase term. Similarly, the term $S(u_2)$ intervenes in that region as two horizontal lines at $u_2=0$ and d. The quantity $S^*(u_1+u_2)$ is represented as the four diagonal broken lines. According to relation (22), lines crossing the origin of the axes have a weight of one while the other lines have a weight of one-third.

Within the fundamental triangle, the product of all these lines leaves only six non-zero points, four of which are on the horizontal axis and simply correspond to Labeyrie's technique

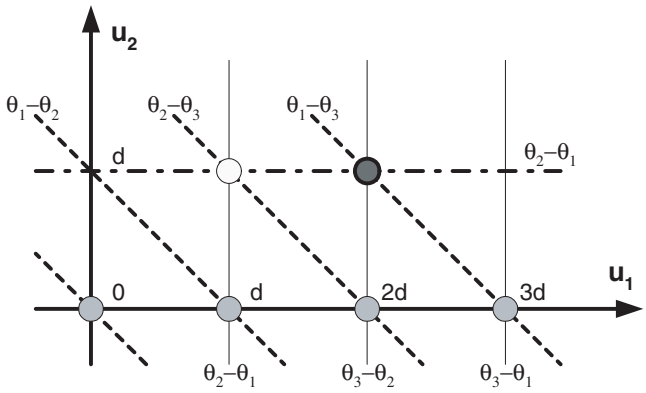

Figure 7. Representation of the bispectrum of an I3T telescope (relation (20)) inside the fundamental triangle. The lines represent the Dirac delta functions that appear in relation (22), with corresponding atmospheric phase terms. These phase terms vanish for the four points on the u_1 axis (at 0, d, $2d$ and $3d$) that correspond to Labeyrie's technique. The point at $\{d, d\}$ remains contaminated by atmospheric phase terms and, on average, its contribution disappears. The point at $\{2d, d\}$ is the phase closure term.

as seen before (figure 5). At the origin of the axes, the bispectrum equals one; at $u_1 = d$, $2d$ and $3d$, its value is one-ninth.

For a single image, the contribution of the point $\{d, d\}$ is proportional to $\exp[\mathrm{i}(3\theta_2 - 2\theta_1 - \theta_3)]$, a non-real quantity that vanishes when the ensemble average is taken. The point at $\{2d, d\}$ corresponds to phase closure; its value is 1/27 (product of three lines of weight one-third). There is a phase closure relation when the angular frequencies involved come from points in the aperture that circularly permute.

This presentation of the I3T telescope can be easily generalized to a full two-dimensional pupil. Making use of relations (5) and (13), the bispectrum may be written as

$$B_s(u_1, u_2) = \langle \int\int\int P(x)P^*(x-u_1)P(y)P^*(y-u_2)P^*(z)P(z-u_1-u_2)\,\mathrm{d}x\,\mathrm{d}y\,\mathrm{d}z \rangle. \tag{23}$$

An illustration of the computations involved by this triple integral is made in figure 8 for the case of a one-dimensional aperture. The representation is made to emphasise closure phase aspects. Within each one-dimensional aperture, the three circles represent the apertures of the I3T described above, with separations d and $2d$. We assume similarly local phase terms θ_1, θ_2 and θ_3 at these three points. The region of the integral that will contribute to the bispectrum is shown between two vertical lines.

For any ordinary relative positions of x, y and z, the integral is zero. For the particular representation of figure 8, where $x = y - u_2$ and $z = y$, the phase terms cancel and the integral is non-zero. The elementary apertures appear in the same phase closure form as for the I3T. For the one-dimensional aperture, the transmission is simply proportional to the length of the telescope minus $u_1 + u_2$.

The alert reader will have noticed that in this computation we have forgotten one term. Indeed, the phase terms cancel also for $y = x - u_1$ and $z = x$. Does it means that in the I3T presentation we forgot a phase closure term? The answer is that the transfer function $S(u)$ of relation (21) is equally given by two telescopes, with separations d and $2d$ or with separations $2d$ and d. There is therefore two pupil configurations leading to similar phase closure. Such reasoning easily generalizes to two-dimensional apertures.

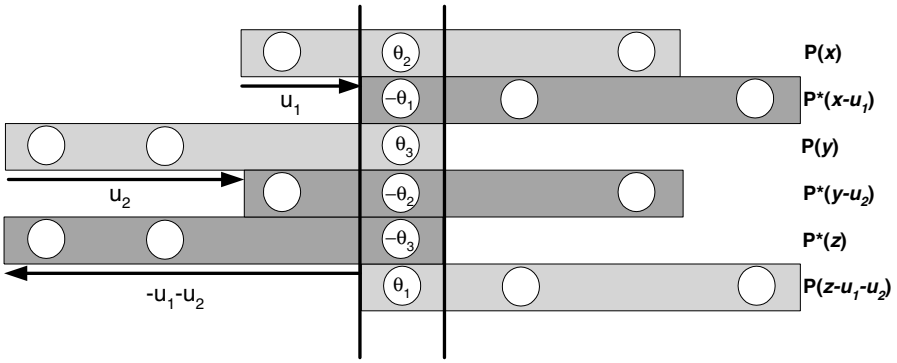

Figure 8. Illustration of $B_S(u_1, u_2)$ for a one-dimensional slit aperture. The rectangles represent the six telescope apertures $P(x)$ to $P(z - u_1 - u_2)$ inside the integral of relation (23). In each slit aperture, the three circles are at positions of the I3T telescope of figure 7, with atmospheric phase values. For any ordinary relative positions of the slit apertures, the integral is zero because phase terms remain uncorrected in the product, as for point $\{d, d\}$ of figure 7. For the particular position represented, in which $x = y - u_2$ and $z = y$, the phase terms cancel and the integral is non-zero, as for the phase closure point $\{2d, d\}$ of figure 7.

6. Analysis in photon counting mode

At very low light levels, speckle patterns are recorded in photon counting mode. The presentation we give here corresponds to the semi-classical theory of the light that uses the theory of wave propagation up to the telescope focus and where the quantum process intervenes only at the sensor. We shall use basic properties of Poisson statistics.

Let us assume that from a classical point of view, the intensity in a given pixel is m photons (m is any real positive number). The number n of photoelectrons actually detected is a positive integer that follows the Poisson statistics of mean m:

$$P(n/m) = \frac{m^n}{n!}\,\mathrm{e}^{-m}. \tag{24}$$

We shall make plenty of use of the factorial moment relationship that relates photodetected and classical moments. Denoting $\langle n^{[k]}\rangle_{\mathrm{P}}$ the factorial moment $\langle n(n-1)\cdots(n-k+1)\rangle_{\mathrm{P}}$, we have

$$\langle n^{[k]}\rangle_{\mathrm{P}} = m^k. \tag{25}$$

This is easily demonstrated as follows:

$$\langle n^{[k]}\rangle_{\mathrm{P}} = \sum_{n=0}^{\infty} \frac{n!}{(n-k)!} P(n/m) = m^k\,\mathrm{e}^{-m} \sum_{n=k}^{\infty} \frac{m^{n-k}}{(n-k)!} = m^k\,\mathrm{e}^{-m} \sum_{j=0}^{\infty} \frac{m^j}{j!} = m^k. \tag{26}$$

Let us assume that we have on average N photoelectrons per frame. From a classical point of view, the intensity in a given pixel for a speckle image $f(r)$ may be written as $m = Nf(r)$. Denoting $f_{\mathrm{p}}(r)$ the photodetected image and substituting $n = f_{\mathrm{p}}(r)$ and $m = Nf(r)$, in relation (25), we can derive for later use the first three moments of $f_{\mathrm{p}}(r)$:

$$\langle f_{\mathrm{p}}(r)\rangle_{\mathrm{P}} = Nf(r) \tag{27a}$$

$$\langle f_{\mathrm{p}}^2(r)\rangle_{\mathrm{P}} = N^2 f^2(r) + Nf(r) \tag{27b}$$

$$\langle f_{\mathrm{p}}^3(r)\rangle_{\mathrm{P}} = N^3 f^3(r) + 3N^2 f^2(r) + Nf(r). \tag{27c}$$

6.1. Photon noise bias in Labeyrie's technique

The ways in which we derive the results are different from the classical Goodman–Belsher approach [18] and are simply based on the fact that the process is a double stochastic process. The photodetected autocorrelation function $C_{\mathrm{p}}(\rho)$ of $f_{\mathrm{p}}(r)$ can be computed using the definition

$$C_{\mathrm{p}}(\rho) = \frac{1}{N^2}\langle \int f_{\mathrm{p}}(r)\, f_{\mathrm{p}}(r+\rho)\, \mathrm{d}r \rangle = \frac{1}{N^2}\langle \int \langle f_{\mathrm{p}}(r)\, f_{\mathrm{p}}(r+\rho)\rangle_{\mathrm{P}}\, \mathrm{d}r\rangle_{\mathrm{S}} \tag{28}$$

where the term N^2 is a normalization factor, which makes the amplitude of $C_p(\rho)$ comparable to that of $C(\rho)$. The ensemble average $\langle\cdots\rangle$ is explicitly split into an average over the photon counting process alone ($\langle\cdots\rangle_{\mathrm{P}}$) and an average over the speckle process ($\langle\cdots\rangle_{\mathrm{S}}$).

First, let us consider the average over the photon counting process alone; we have

$$\begin{aligned} \rho \neq 0 \qquad & \langle f_{\mathrm{p}}(r)\, f_{\mathrm{p}}(r+\rho)\rangle_{\mathrm{P}} = \langle f_{\mathrm{p}}(r)\rangle_{\mathrm{P}} \langle f_{\mathrm{p}}(r+\rho)\rangle_{\mathrm{P}} = N^2 f_{\mathrm{p}}(r)\, f(r+\rho) \\ \rho = 0 \qquad & \langle f_{\mathrm{p}}^2(r)\rangle_{\mathrm{P}} = N^2 f^2(r) + N f(r) \end{aligned} \tag{29}$$

where for $\rho \neq 0$, the quantities $f_{\mathrm{p}}(r)$ and $f_{\mathrm{p}}(r+\rho)$ are independent RVs for the Poisson process. Substituting relations (29) in (28) and making use of the Dirac delta function $\delta(\rho)$ to deal with the different values of ρ, we can write

$$C_{\mathrm{p}}(\rho) = C(\rho) + \frac{\delta(\rho)}{N}. \tag{30}$$

The Wiener–Khinchin theorem remains valid for the photodetected image, and the power spectrum is readily obtained by a Fourier transform:

$$W_{\mathrm{p}}(u) = W(u) + \frac{1}{N}. \tag{31}$$

The photodetected power spectrum $W_{\mathrm{p}}(u)$ is biased by a term $1/N$, which has to be subtracted. In practice this is not easy since we never have access to an ensemble average involving an infinite number of frames, but only to a finite number, K, of frames. Invoking the central limit theorem, the noise then fluctuates around its expected level with a root mean square (RMS) of $1/(N\sqrt{K})$. A simulation of what can be obtained at photoelectron counting levels for a double-star speckle pattern is shown in figure 9.

It is interesting to note that it is possible to perform an unbiased experiment using the cross spectrum instead of the power spectrum. For that we need to record two simultaneous images of $f_{\mathrm{p}}(r)$ (we may use a semi-transparent glass for such a purpose). Let $f_{\mathrm{p}1}(r)$ and $f_{\mathrm{p}2}(r)$ be these images, each with N_1 and N_2 photoelectrons per image on average. Independently of the value of ρ, we can write

$$\begin{aligned} C_{\mathrm{p}12}(\rho) &= \frac{1}{N_1 N_2}\langle \int \langle f_{\mathrm{p}1}(r)\, f_{\mathrm{p}2}(r+\rho)\rangle_{\mathrm{P}}\, \mathrm{d}r\rangle_{\mathrm{S}} = \frac{1}{N_1 N_2}\langle \int \langle f_{\mathrm{p}1}(r)\rangle_{\mathrm{P}} \langle f_{\mathrm{p}2}(r+\rho)\rangle_{\mathrm{P}}\, \mathrm{d}r\rangle_{\mathrm{S}} \\ &= \langle \int f(r)\, f(r+\rho)\, \mathrm{d}r\rangle_{\mathrm{S}} = C(\rho) \end{aligned} \tag{32}$$

where we have used the independence of photon noise of $f_{\mathrm{p}1}(r)$ and $f_{\mathrm{p}2}(r)$, since they consist of different photoelectrons. The Fourier transform of $C_{\mathrm{p}12}(\rho)$ gives the cross-spectrum unbiased estimate of the power spectrum. For real measurements, made on a finite number of images, the cross spectrum appears as a complex quantity, whose non real-positive part is due to insufficient averaging. The drawback of this technique is that the equivalent number of photons per frame is half that for the regular speckle technique.

6.2. Photon noise bias in Weigelt's technique

A similar computation can be applied for the computation of the photodetected triple correlation function. We have

$$T_{\mathrm{p}}(\rho_1, \rho_2) = \frac{1}{N^3}\langle \int \langle f_{\mathrm{p}}(r)\, f_{\mathrm{p}}(r+\rho_1)\, f_{\mathrm{p}}(r+\rho_2)\rangle_{\mathrm{P}}\, \mathrm{d}r\rangle_{\mathrm{S}}. \tag{33}$$

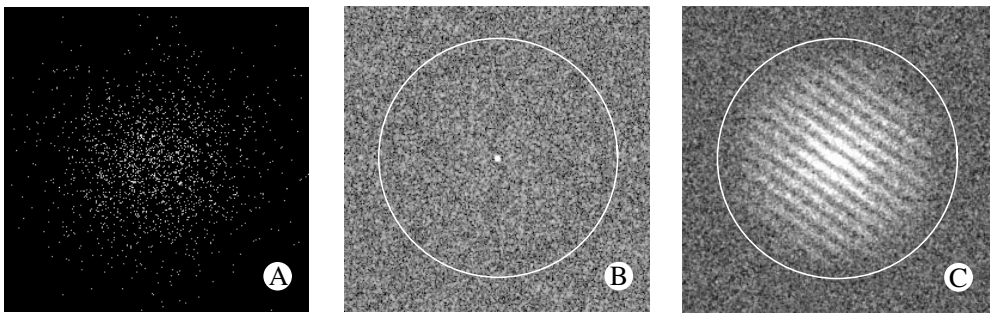

Figure 9. Simulation of a speckle interferometry experiment at photo-counting levels. It closely follows the semi-classical theory described. A speckle image representing the classical intensity is computed first. Then the intensity obtained for each point (any non-negative number) is taken as the mean value of a Poisson distribution whose outcome is a random integer number. The total number of photons per frame (2000 in this simulation) varies from image to image. (A) Example of a photodetected image of a double star speckle pattern. The corresponding ETF $|F_{\mathrm{p}}(u)|^2$ estimated from (B) a single image and (C) 100 images. The circle represents the telescope cut-off frequency. The stars are of comparable intensities; the detection would be more difficult for large differences. Processing a very large number of images is mandatory to obtain good results in speckle interferometry techniques.

Bias terms are present when at least two of the variables inside the photon average are the same. This occurs for $\rho_1 = \rho_2 = 0$, $\rho_1 = 0$, $\rho_2 = 0$ and $\rho_1 = \rho_2$. We have

$$\langle f_{\mathrm{p}}(r) f_{\mathrm{p}}(r+\rho_1) f_{\mathrm{p}}(r+\rho_2)\rangle_{\mathrm{P}}$$
$$= \begin{cases} \langle f_{\mathrm{p}}^3(r)\rangle_{\mathrm{p}} = N^3 f^3(r) + 3N^2 f^2(r) + N f(r) & \rho_1 = \rho_2 = 0 \\ \langle f_{\mathrm{p}}^2(r)\rangle_{\mathrm{P}} \langle f_{\mathrm{p}}(r+\rho_2)\rangle_{\mathrm{P}} = N^3 f^2(r) f(r+\rho_2) + N^2 f(r) f(r+\rho_2) & \rho_1 = 0;\ \rho_2 \neq 0 \\ \langle f_{\mathrm{p}}^2(r)\rangle_{\mathrm{P}} \langle f_{\mathrm{p}}(r+\rho_1)\rangle_{\mathrm{P}} = N^3 f^2(r) f(r+\rho_1) + N^2 f(r) f(r+\rho_1) & \rho_1 \neq 0;\ \rho_2 = 0 \\ \langle f_{\mathrm{p}}(r)\rangle_{\mathrm{P}} \langle f_{\mathrm{p}}^2(r+\rho_1)\rangle_{\mathrm{P}} = N^3 f(r) f^2(r+\rho_1) + N^2 f(r) f(r+\rho_1) & \rho_1 = \rho_2 \neq 0 \\ \langle f_{\mathrm{p}}(r)\rangle_{\mathrm{P}} \langle f_{\mathrm{p}}(r+\rho_2)\rangle_{\mathrm{P}} \langle f_{\mathrm{p}}(r+\rho_2)\rangle_{\mathrm{P}} = N^3 f(r) f(r+\rho_1) f(r+\rho_2) & \rho_1 \neq \rho_2 \neq 0. \end{cases} \tag{34}$$

Making use of the Dirac delta functions $\delta(\rho_1)$, $\delta(\rho_2)$ and $\delta(\rho_2 - \rho_1)$, we can summarize these conditions as

$$T_{\mathrm{p}}(\rho_1, \rho_2) = T(\rho_1, \rho_2) + \frac{1}{N}\delta(\rho_1) C(\rho_2) + \frac{1}{N}\delta(\rho_2) C(\rho_1) + \frac{1}{N}\delta(\rho_2 - \rho_1) C(\rho_1) + \frac{1}{N^2}\delta(\rho_1)\delta(\rho_2). \tag{35}$$

The photodetected triple correlation is biased by a term in $1/N^2$ at the origin and terms proportional to the autocorrelation function for the axes ($\rho_1 = 0$, $\rho_2 = 0$) and the first bisector ($\rho_1 = \rho_2$) in the geometrical representation of a one-dimensional signal.

The photodetected bispectrum is the Fourier transform of this relation. We obtain

$$B_{\mathrm{p}}(u_1, u_2) = \mathfrak{F}_1\mathfrak{F}_2[C_{\mathrm{p}}(\rho_1, \rho_2)] = B(u_1, u_2) + \frac{1}{N}\{W(u_1) + W(u_2) + W(u_1 + u_2)\} + \frac{1}{N^2} \tag{36}$$

where the term $W(u_1 + u_2)$ comes from the following application of Fourier operators

$$\mathfrak{F}_1\mathfrak{F}_2\left[\frac{1}{N}\delta(\rho_2 - \rho_1) C(\rho_1)\right] = \frac{1}{N}\mathfrak{F}_1[C(\rho_1)\mathfrak{F}_2[\delta(\rho_2 - \rho_1)]] = \frac{1}{N}\mathfrak{F}_1[C(\rho_1)\,\mathrm{e}^{-2\mathrm{i}\pi\rho_1 u_2}]$$
$$= \frac{1}{N} W(u_1 + u_2). \tag{37}$$

A constant term and terms proportional to the power spectrum bias the bispectrum. As for the autocorrelation analysis, it is possible to obtain an unbiased estimate by computing the bispectrum from photon-noise independent records of the same speckle image. This will of course be obtained at the expenses of a larger variance of the result. Estimating these variances [19] is a much tougher task and one that will not be presented here.

7. Conclusions

The presentation of the speckle techniques we have given in this paper is obviously not exhaustive, and must be considered as an introduction to the subject. It is part of a course given at the University of Nice Sophia-Antipolis (France) for graduate students.

Emphasis is made on mathematical aspects that may easily give rise to theoretical examinations. In the main the techniques of Labeyrie and Weigelt are detailed. The technique of Knox and Thompson is briefly outlined. Due to lack of space, many other techniques such as 'shift-and-add' [4], differential speckle interferometry [20], probability imaging [21] and dark speckle [22, 23] have not been considered. From a practical point of view, it would have been interesting to go into more detail of a practical experiment, from detection problems encountered with a photocounting camera to the actual processing of real data. The way in which these techniques may be applied to solar observations would also be of interest. This would have doubled the length of the paper.

The originality of the presentation lies in the way known results are shown. This includes various points of different importance, such as the way in which one may easily simulate perturbed wavefronts and corresponding speckle patterns, manipulate Fourier transforms and ensembles averages or show relationships between the bispectrum and the other techniques, including phase closure. The treatment of the photo-detection process, using the semi-classical theory, Poisson statistics and factorial moments is very simple, and may be used for other low-light level experiments.

The computational techniques presented here may be of interest outside the astrophysical domain, in particular in signal and image processing. The demonstration of the Wiener–Khinchin theorem and its generalization to the bispectrum is a more condensed version of what is generally given in the literature. The use of plane transformation operators for the geometrical presentation of the full recovery of the bispectrum from the fundamental triangle is also easy to manipulate. These approaches easily generalize to higher-order moments, such as the trispectrum.

References

[1] Labeyrie A 1976 High resolution techniques in optical astronomy *Progress in Optics* vol XIV, ed E Wolf (Amsterdam: North-Holland) pp 49–87
[2] Fried D L 1966 *J. Opt. Soc. Am.* **56** 1372–9
[3] Roddier F 1981 The effects of atmospheric turbulence in optical astronomy *Progress in Optics* vol XIX, ed E Wolf (Amsterdam: North-Holland) pp 281–376
[4] Bates R H T 1982 Astronomical speckle imaging *Phys. Rep.* **90** 203–97
[5] Roddier F 1988 Interferometric imaging in optical astronomy *Phys. Rep.* **170** 97–166
[6] Knox K T and Thompson B J 1974 *Astron. J.* **193** L45–8
[7] Weigelt G 1991 Triple correlation imaging in optical astronomy *Progress in Optics* vol XXIX, ed E Wolf (Amsterdam: North-Holland) pp 295–319
[8] Roddier F 1999 *Adaptive Optics in Astronomy* (Cambridge: Cambridge University Press)
[9] Wolfram S 1999 *The Mathematica Book* 4th edn (Cambridge: Cambridge University Press)
[10] Ziad A, Borgnino J, Agabi A and Martin F 1992 *J. Opt. (Paris)* **23** 131–42
[11] Goodman J W 1968 *Introduction to Fourier Optics* (New York: McGraw-Hill)
[12] Fienup J R 1978 *Opt. Lett.* **3** 27–9
[13] Lohmann A W, Weigelt G and Wirnitzer B 1983 *Appl. Opt.* **22** 4028–37
[14] Bartelt H, Lohmann A W and Wirnitzer B 1984 *Appl. Opt.* **23** 3121–9
[15] Barakat R and Ebstein S 1987 *J. Opt. Soc. Am.* A **4** 1756–63
[16] Ayers G R, Northcott M J and Dainty J C 1988 *J. Opt. Soc. Am.* A **5** 963–85

[17] Roddier F 1986 *Opt. Commun.* **60** 145–8
[18] Goodman J W 1985 *Statistical Optics* (New York: Wiley)
[19] Aime C 1997 *Pure Appl. Opt.* **6** 1–14
[20] Petrov R G, Balega Y Y, Blazit A, Vassyuk V V, Lagarde S and Foy R 1996 *Astron. Lett.* **22** 348–53
[21] Aime C, Ricort G and Perrier C 1990 *Exp. Astron.* **1** 267–84
[22] Labeyrie A 1995 *Astron. Astrophys.* **298** 544–8
[23] Aime C 2000 *J. Opt. A: Pure Appl. Opt.* **2** 411–21